Dynamical tunneling-assisted coupling of high-Q deformed microcavities using a free-space beam

Qi-Fan Yang,* Xue-Feng Jiang, Ya-Long Cui, Linbo Shao, and Yun-Feng Xiao†
State Key Lab for Mesoscopic Physics and School of Physics, Peking University, People's Republic of China
(Received 26 March 2013; published 7 August 2013)

We investigate the efficient free-space excitation of high-Q resonance modes in deformed microcavities via dynamical tunneling-assisted coupling. A quantum scattering theory is employed to study the free-space transmission properties, and it is found that the transmission includes the contribution from (1) the off-resonance background and (2) the on-resonance modulation, corresponding to the absence and presence of high-Q modes, respectively. The theory predicts asymmetric Fano-like resonances around high-Q modes in background transmission spectra, which are in good agreement with our recent experimental results. Dynamical tunneling across Kolmogorov-Arnold-Moser tori, which plays an essential role in the Fano-like resonance, is further studied. This efficient free-space coupling holds potential advantages to simplify experimental conditions and excite high-Q modes in higher-index-material microcavities.

DOI: 10.1103/PhysRevA.88.023810 PACS number(s): 42.60.Da, 42.55.Sa, 42.25.−p, 42.79.Gn

I. INTRODUCTION

Over the last two decades, optical whispering-gallery-mode (WGM) microresonators (or microcavities) [1] with high quality factors and small mode volumes have promised laboratory-on-a-chip applications ranging from fundamental physics to various photonic devices, such as nonlinear optics [2–5], cavity quantum electrodynamics [6–8], cavity optomechanics [9–11], low-threshold microlasers [12–15], and highly sensitive optical biosensors [16–20]. In these applications, traditionally light is coupled into the WGM microcavities by evanescent couplers, such as prisms [21], tapered fibers [22,23], and angle-polished fibers [24], which have been validated to be highly efficient. In all of these coupling configurations, the microcavities are typically separated from the couplers by a distance of subwavelength because the evanescent fields of WGMs extend over a very short range. The use of the evanescent couplers, however, is not suitable in some important applications. For example, a higher-index-material microcavity [4,25] cannot be efficiently excited by the tapered fiber due to phase mismatching. In addition, the external couplers degrade high-Q factors (defined as $\omega\tau$, where ω denotes the photon frequency and τ is its intracavity lifetime) in the case of the overcoupling regime, and they are not convenient in low-temperature chambers.

It has been demonstrated that WGMs in a specially designed deformed cavity can be directly excited by a free-space optical beam [26,27]. This direct free-space coupling is of importance because it is robust and requires less rigorous experimental conditions than the evanescent couplers mentioned above. This efficient free-space coupling originates from the breaking of rotational symmetry in deformed microcavities, which produces a highly directional emission assisted by the dynamical tunneling, different from the isotropic nature of a circular WGM cavity [26–29]. According to the time reversion, i.e., the reversibility of light path, free-space beams at certain positions are expected to couple into the high-Q modes via chaotic modes when they are on-resonance. So far, this type of free-space coupling technique has been demonstrated experimentally to reach a resonant efficiency exceeding 50% [30]. A straightforward method to characterize free-space coupling is to study its transmission property, e.g., transmission spectrum. In this paper, we investigate the dynamical tunneling properties between the chaotic modes and the regular modes in detail, and predict transmission spectra of the free-space coupling by employing a quantum scattering theory. It is found that the spectrum can behave asymmetrically as a Fano-like line shape [31], in good agreement with our recent experimental observation [32].

This paper is organized as follows. In Sec. II, we present the mechanism of dynamical tunneling-assisted coupling and introduce a quantum scattering theory to predict a general transmission in free space. It is found that the free-space transmission spectrum includes the contribution from both the off-resonance background and the on-resonance modulation. In Sec. III, we study the off-resonance background transmission in the absence of the high-Q regular mode, corresponding to the unperturbed scattering. The off-resonance background transmission spectrum shows periodic modulations, which is in good agreement with both the numerical simulation and experimental results. In Sec. IV, the on-resonance transmission spectra are studied in detail. It is revealed that they depend strongly on (i) the additional phase when light travels in chaos trajectories and (ii) the rate of dynamical tunneling. Section V rigourously explains the chaotic states and the coupling strength, with which we deduce the condition of highest excitation efficiency. Section VI further investigates the Kolmogorov-Arnold-Moser (KAM) barriers, which are predominant in the dynamical tunneling process. Section VII is a short summary of the paper.

II. DYNAMICAL TUNNELING-ASSISTED COUPLING

Without loss of generality, here we consider a two-dimensional deformed cavity made of silica with refractive index $n = 1.45$ as shown in Fig. 1, which has the boundary

*Present address: T. J. Watson Laboratory of Applied Physics, California Institute of Technology, Pasadena, California 91125, USA; qfyang@caltech.edu
†www.phy.pku.edu.cn/∼yfxiao/index.html

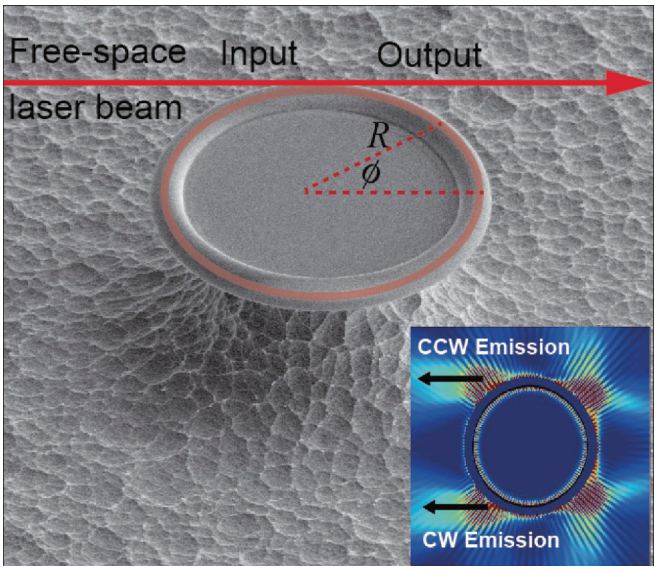

FIG. 1. (Color online) Scanning electron microscope (SEM) view of a deformed silica microtoroid cavity. Here R and ϕ are the polar coordinates in the cavity plane. The red arrow denotes the laser beam. Inset: False color illustration of a resonant mode distribution obtained with wave simulation. The two black arrows denote the dominantly directional emission toward the 180° far-field direction. The strength outside the cavity is magnified for a clear view.

defined in polar coordinates as

$$R(\phi) = \begin{cases} R_0\left(1+\eta\sum_{i=2,3}a_i\cos^i\phi\right) & \text{for } \cos\phi \geqslant 0 \\ R_0\left(1+\eta\sum_{i=2,3}b_i\cos^i\phi\right) & \text{for } \cos\phi < 0, \end{cases} \quad (1)$$

where R_0 and η represent size and deformation parameters, respectively. Cavity shape parameters are set as $a_2 = -0.1329$, $a_3 = 0.0948$, $b_2 = -0.0642$, and $b_3 = -0.0224$. When $\eta = 1$, a highly directional far-field universal pattern of high-Q modes has been predicted [33] and demonstrated experimentally [34]. This emission characteristic is clearer by plotting the near-field pattern, as shown in the inset of Fig. 1. It can be seen that the two major emission positions are at $\phi = \pi/2$ and $3\pi/2$, corresponding to refractive escape from counterclockwise (CCW) and clockwise (CW) modes, respectively. Thus, we expect that in a time-reversed way, an excitation beam focused on the primary emission position at $\phi = \pi/2$, as shown in Fig. 1, can eventually excite the CW resonant modes. To quantitatively study this chaos-assisted process, we use a quantum scattering theory to model the transmission, from which the coupling characteristic of the high-Q modes can be obtained.

Before studying the transmission spectrum, we first present the mechanism of dynamical tunneling-assisted coupling. The Poincaré surface of section (PSOS) provides a simple and intuitive way to model the ray dynamics in deformed microcavities by recording the angular position ϕ and the incident angle χ of the rays, similar to billiards in quantum chaos. Except for an ellipse-shaped cavity, the deformed microcavity has a mixed phase space including three types of structures: KAM tori, islands, and chaos sea, corresponding to quasiperiodicity, periodicity, and chaos motion of ray trajectories [35], respectively, as shown in Fig. 2(a). KAM tori separate the PSOS into disjoint regions. As shown in

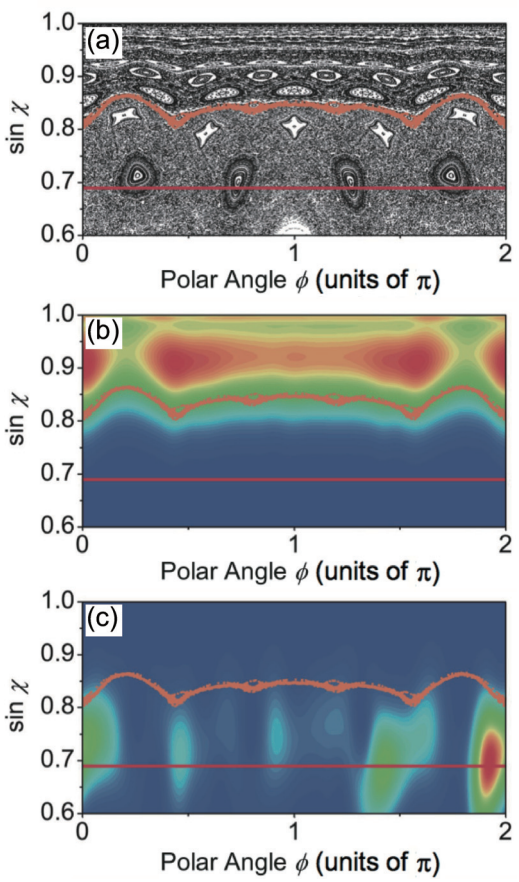

FIG. 2. (Color online) (a) A typical PSOS of the deformed microcavity. The red solid line denotes the critical line defined as $\sin\chi = 1/n$. The orange dotted line stands for a KAM torus. (b), (c) Normalized Husimi projection of the resonant mode and the excitation state, respectively.

Fig. 2(b), high-Q modes are usually localized in the regular regions bounded by a KAM torus [36–38]. For such a localized high-Q mode, the excitation by a free-space beam is primarily attributed to two channels: (i) *angular momentum tunneling* and (ii) *dynamical tunneling via chaos* [39]. It has been demonstrated that the dynamical tunneling dominates, since the lifetime of photons that refract into the deformed cavity greatly increases along chaotic trajectories [26].

In the system consisting of a microcavity and unbounded medium outside, the state $|\psi_\omega\rangle$ which describes the electromagnetic field excited by the incident beam satisfies the stationary Schrödinger equation

$$H\,|\psi_\omega\rangle = \omega\,|\psi_\omega\rangle\,, \quad (2)$$

where H stands for the system Hamiltonian. As mentioned above, not only chaotic modes but also the regular mode can be excited by an appropriate free-space beam thanks to the dynamical tunneling. This can be demonstrated by plotting the Husimi projection [40] of the excitation state $|\psi_\omega\rangle$, as shown in Fig. 2(c). Thus $|\psi_\omega\rangle$ can be expanded as a linear combination of chaotic mode $|C_\omega\rangle$ and regular mode $|\mathrm{WGM}\rangle$ [41], with the form

$$|\psi_\omega\rangle = a_\omega|\mathrm{WGM}\rangle + \int d\omega' b_\omega(\omega')|C_{\omega'}\rangle, \quad (3)$$

where a_ω and $b_\omega(\omega')$ are weight coefficients of these states at frequency ω. Throughout this paper, we use regular mode and chaotic mode to describe uncoupled states, and dynamical tunneling is the interaction between an uncoupled regular mode and uncoupled chaotic modes. The system Hamiltonian satisfies

$$\langle \mathrm{WGM}|H|\mathrm{WGM}\rangle = \omega_0 - i\gamma/2, \tag{4a}$$

$$\langle C_{\omega'}|H|C_\omega\rangle = \omega\delta(\omega' - \omega), \tag{4b}$$

$$\langle C_\omega|H|\mathrm{WGM}\rangle = V_\omega. \tag{4c}$$

Here ω_0 and ω are the frequencies of the resonant regular mode and the incident light, respectively. The coupling coefficient between $|C_\omega\rangle$ and $|\mathrm{WGM}\rangle$, governed by the dynamical tunneling, is described by V_ω. The decay rate γ consists of the intrinsic loss and the chaos-assisted tunneling loss. In detail, the intrinsic decay rate γ_0 is attributed to radiation, material absorption, and scattering losses in the cavity, while the chaos-assisted decay rate γ_1 describes tunneling into the chaotic modes other than $|C_\omega\rangle$. We denote them as $|C_\omega^\perp\rangle$.

In this paper, we consider the chaotic modes as a continuum and use a standard quantum scattering model to interpret the transmission line shape. Here we assume that $|C_\omega\rangle$ and $|\mathrm{WGM}\rangle$ are orthogonal [42]. By substituting Eq. (3) into Eq. (2), the coefficients a and b are determined by

$$(\omega_0 - i\gamma/2)a_\omega + \int d\omega' V_{\omega'}^* b_\omega(\omega') = \omega a_\omega, \tag{5a}$$

$$V_{\omega'} a_\omega + \omega' b_\omega(\omega') = \omega b_\omega(\omega'). \tag{5b}$$

On one hand, applying a standard treatment [31], the coefficient b yields

$$b_\omega(\omega') = \left[\frac{1}{\omega - \omega'} + z_\omega\delta(\omega - \omega')\right] V_{\omega'} a_\omega, \tag{6}$$

where

$$z_\omega = \frac{\omega - \omega_0 + i\gamma/2 - F(\omega)}{|V_\omega|^2}. \tag{7}$$

The shift of resonant frequency is expressed as $F(\omega) = \mathrm{P}\int \kappa/[2\pi(\omega - \omega')]d\omega'$, where P denotes Cauchy's principal value. The reduced coupling strength κ between $|C_\omega\rangle$ and $|\mathrm{WGM}\rangle$ is obtained through the Fermi golden rule under the first Markov approximation [43], with

$$\kappa = 2\pi|V_\omega|^2. \tag{8}$$

For the high-Q mode in a slightly deformed cavity whose intrinsic linewidth γ is orders of magnitude smaller than the resonant frequency ω_0, the bounds of the integral of $F(\omega)$ can be extended to infinity, resulting in

$$F(\omega) = \frac{\kappa}{2\pi}\mathrm{P}\int_{-\infty}^{+\infty} d\omega' \frac{1}{\omega - \omega'} = 0. \tag{9}$$

On the other hand, the normalization condition $\langle\psi_{\omega'}|\psi_\omega\rangle = \delta(\omega' - \omega)$ determines the value of a by

$$|a_\omega|^2|V_\omega|^2[\pi^2 + |z_\omega|^2]\delta(\omega' - \omega) + a_{\omega'}^* a_\omega \frac{i\gamma_0}{\omega' - \omega} = \delta(\omega' - \omega). \tag{10}$$

By integrating this equation over ω, we have

$$|a_\omega|^2 = \frac{1}{2\pi}\frac{\kappa}{(\omega - \omega_0)^2 + \left(\frac{\gamma+\kappa}{2}\right)^2}. \tag{11}$$

In Eq. (11), $|a_\omega|^2$ describes the excitation probability by the free-space beam, from which we can deduce that the FWHM (full width at half maximum) of the regular mode is expressed as $\kappa + \gamma \equiv \gamma_t$. It should be noted that γ_t remains unchanged when the free-space coupling efficiency changes [27], while in fiber taper coupling the total decay rate will vary.

Finally, the transmission spectrum is calculated as

$$\begin{aligned} T(\omega) &= |\langle\psi_\omega|S|\mathrm{in}\rangle|^2 \\ &= |a_\omega|^2|\langle \mathrm{WGM} + \mathrm{P}\int d\omega' \frac{V_{\omega'}}{\omega - \omega'} C_{\omega'} \\ &\quad + \frac{(\omega - \omega_0 + i\gamma/2)V_\omega}{|V_\omega|^2} C_\omega|S|\mathrm{in}\rangle|^2, \end{aligned} \tag{12}$$

where S is a suitable transmission operator connecting $|\mathrm{in}\rangle$ and $|C_\omega\rangle$, and $|\langle C_\omega|S|\mathrm{in}\rangle|^2$ describes the probability of the transmitted signal [31]. To get a more general expression, we introduce a dimensionless frequency detuning defined by $\epsilon \equiv (\omega - \omega_0)/(\kappa/2)$ and the ratio $K \equiv \gamma/\kappa = (\gamma_t - \kappa)/\kappa$. Therefore, the transmission is simplified to

$$T(\omega) = \frac{|q_\omega + \epsilon - iK|^2}{(1 + K)^2 + \epsilon^2}|\langle C_\omega|S|\mathrm{in}\rangle|^2. \tag{13}$$

Here q_ω represents the crucial line-shape parameter of the transmission spectrum $T(\omega)$, taking the form

$$q_\omega = \frac{\langle\varphi_\omega|S|\mathrm{in}\rangle}{\pi V_\omega^*\langle C_\omega|S|\mathrm{in}\rangle}, \tag{14}$$

where $|\varphi_\omega\rangle = |\mathrm{WGM}\rangle + \mathrm{P}\int d\omega' \frac{V_{\omega'}|C_{\omega'}\rangle}{\omega - \omega'}$. To give a clear understanding, we consider two extreme cases.

(i) In classical mechanics where dynamical tunneling is forbidden, the regular mode cannot be excited. Thus there is no interaction between the regular mode and the chaotic mode ($\kappa \to 0$), and the coefficients $\epsilon, K \propto 1/\kappa$ as well as $q_\omega \propto 1/\sqrt{\kappa}$. In this case, the transmission spectra yields to

$$T_0(\omega) = |\langle C_\omega|S|\mathrm{in}\rangle|, \tag{15}$$

which can be regarded as the unperturbed scattering. In Sec. III, we will discuss the unperturbed scattering, which is of importance for the line-shape near resonance.

(ii) In the ideal condition, the regular mode is excited by a phase conjugation wave of its emission pattern. If its intrinsic loss is negligible, which indicates that $\gamma \ll \kappa$ and $K \to 0$, the regular mode is "complete excited" (see Sec. V). In such condition, the transmission yields a standard Fano resonance,

$$T(\omega) = \frac{|q_\omega + \epsilon|^2}{1 + \epsilon^2}|\langle C_\omega|S|\mathrm{in}\rangle|^2. \tag{16}$$

III. OFF-RESONANCE TRANSMISSION

We now investigate the background scattering in the absence of the high-Q regular mode. It has been reported that nonresonant pumping in a deformed microcavity can be well modeled by ray dynamics [44,45]. In our case, the unperturbed transmission is studied in wave optics, and

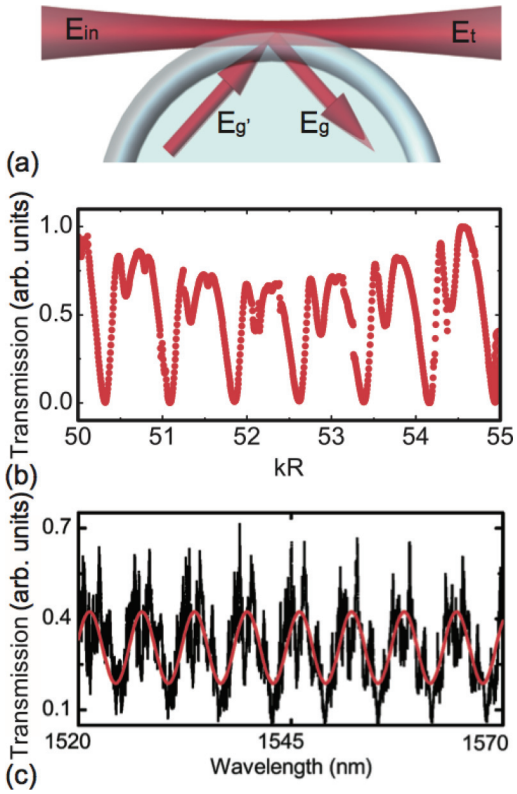

FIG. 3. (Color online) (a) The schema of the scattering process described by Eq. (17). (b) Stimulated transmission spectrum of the free-space excitation process obtained by the boundary element method. (c) Experimental spectrum (black) and the fitted oscillations (red).

it results from the interference between two components, according to the schema shown in Fig. 3(a): (i) the direct transmitted amplitude E_t and (ii) the contribution from the dissipated amplitude $E_{g'}$ via diffusing inside the cavity. To give a clear picture of the interference, we apply the transmission matrix, and the amplitudes are indicated by

$$\begin{pmatrix} E_t \\ E_g \end{pmatrix} = \begin{pmatrix} t & g' \\ g & t' \end{pmatrix} \begin{pmatrix} E_{in} \\ E_{g'} \end{pmatrix}. \tag{17}$$

The intracavity fields $E_{g'}$ and E_g are related by

$$E_{g'} = \alpha E_g, \tag{18}$$

where α is a coefficient including the loss and the phase change in a round trip. The transition matrix element is then given by

$$\begin{aligned} \langle C_\omega | S | \text{in} \rangle &= \frac{E_t}{E_{in}} = t + \frac{\alpha g' g}{1 - \alpha t'} \\ &= t + r e^{i\theta}. \end{aligned} \tag{19}$$

Here r and θ can be understood as the equivalent amplitude factor and phase difference of the forward-emitted field from the cavity, respectively. Hence, the unperturbed transmission takes the form

$$T_0 = |\langle C_\omega | S | \text{in} \rangle|^2 = r^2 \left[1 + \left(\frac{t}{r} \right)^2 + 2 \frac{t}{r} \cos\theta \right]. \tag{20}$$

In a wide frequency width, the phase difference θ can be simplified as nkL_{eff}, with L_{eff} representing the equivalent chaotic path length of the light inside the cavity. Thus the transmission spectrum shows periodic modulations, in good agreement with the numerically simulated transmission, as shown in Fig. 3(b). In experiment, we focus the incident beam on the periphery of a deformed microtoroid with the principle radius 45 μm and the waist of the beam about 3 μm [34]. Figure 3(c) reveals that the experimentally detected transmission also oscillates periodically. Note that the narrow fluctuations in the transmission are due to the Fabry-Perot oscillations between two lenses. From experimental results, the ratio t/r and L_{eff} can be obtained by fitting the large-scale transmission, as shown in red in Fig. 3(c). In the situation of Fig. 3(c), $t/r = 0.16$ and L_{eff} is about 262.35 μm, while the cavity size $R_0 = 45$ μm.

IV. ON-RESONANCE TRANSMISSION

We turn to the study of the on-resonance transmission. It is noted that the direct excitation probability of high-Q regular modes via an evanescent field is negligible due to angular momentum mismatch. Thus the amplitude $\langle \text{WGM} | S | \text{in} \rangle$ has a minor contribution to the transmission. In this case, the line-shape parameter q can be reduced to a simplified form. By substituting Eq. (19) into Eq. (14), we obtain the expression of the line-shape parameter,

$$q_\omega = \frac{\mathrm{P} \int d\omega' \frac{1}{\omega - \omega'} V_{\omega'}^* \langle C_{\omega'} | S | \text{in} \rangle}{\pi V_\omega^* \langle C_\omega | S | \text{in} \rangle} = -\frac{i e^{i\theta}}{t/r + e^{i\theta}}, \tag{21}$$

where $\theta = nkL_{\text{eff}}$, as mentioned above. By substituting Eq. (21) into Eq. (13), the on-resonance transmission can be deduced. In the following, we will show that the line shape of the transmission spectrum is determined by q_ω, which primarily depends on θ, while the modulation depth relies on the relative coupling strength described by K.

Figures 4(a)–4(h) plot calculated transmission spectra against the phase difference θ, which experience symmetric Lorentz absorption dips, asymmetric Fano-like line shapes, and symmetric electromagnetically-induced-transparency (EIT)-like peaks as θ varies from 0 to 2π. From Fig. 3(a), the transmission is a result of interference between two components: the direct transmitted light and the emitted light from the cavity, and θ actually describes the phase difference between them. Interestingly, the on-resonance transmission appears as a symmetric dip on the background where the two components constructively interfere [$\theta = 0$ in Fig. 4(a)], while it switches to an EIT-like peak when they destructively interfere [$\theta = \pi$ in Fig. 4(e)]. This is because when on-resonance, the chaotic modes refractively excited by the incident beam can couple to the regular mode via dynamical tunneling, which results in a phase shift as energy couples back to the chaotic modes. Hence, although the background components constructively (destructively) interfere, such counteraction adds a destructive modulation to the chaotic modes, reflecting a dip (peak) on the transmission.

In experiment, we have observed such Fano resonance as predicted in this paper. As shown in Figs. 5(a) and 5(b), high-Q modes can lead to EIT-like peaks and asymmetric Fano resonances on the transmission spectra. As discussed above,

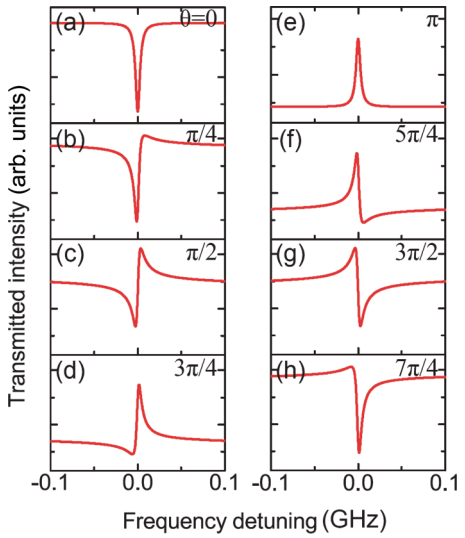

FIG. 4. (Color online) Calculated transmission spectra with $\kappa/2\pi, \gamma/2\pi = 0.003$ GHz and $t/r = 0.2$. The phase shift between the two amplitudes varies from 0 to $7\pi/4$.

the Fano-resonance transmission spectra can be regarded as the modulation of the high-Q mode on the off-resonance background. Such modulation depends strongly on the coupling strength κ between the chaotic modes and the regular mode according to Eq. (13). Here we study the two special cases: EIT-like line shapes and Lorentz dips. As shown in the solid curve in Fig. 6(a), the modulation of the regular mode to the transmission spectrum is minor when $K = 60$. In this case, the excitation probability is extremely low. As K decreases (i.e., the dynamical tunneling is enhanced), the height of the EIT peak increases monotonically, where the off-resonance backgrounds are lifted to the same level. When the loss described by $\gamma_0 + \gamma_1$ is negligible compared with the coupling strength κ, i.e., $K \to 0$, the EIT peak reaches its maximum. Similarly, Fig. 6(b) shows that the

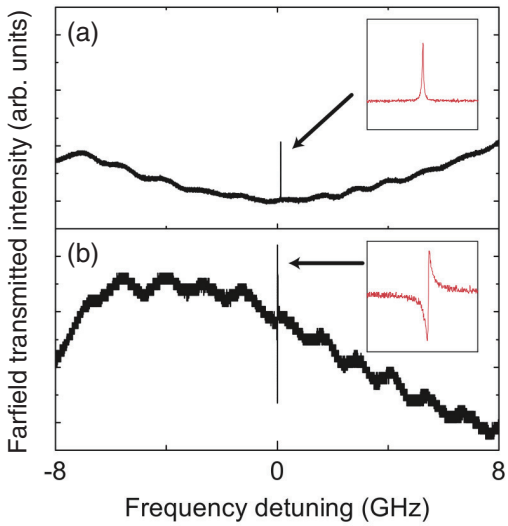

FIG. 5. (Color online) Experimental transmission spectra. The on-resonance line shapes are (a) EIT-like and (b) asymmetric Fano resonance. Insets: Enlarged views of the on-resonance transmission.

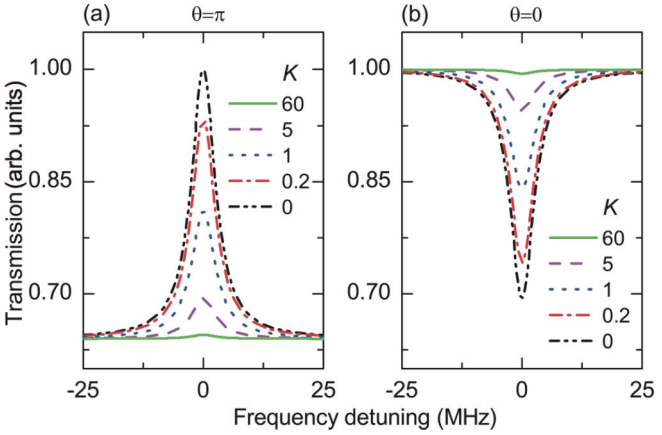

FIG. 6. (Color online) Calculated transmission spectra with $\gamma_t/2\pi = 0.006$ GHz and $t/r = 0.2$, and with K varying from 0 to 60, for (a) EIT-like line shape and (b) Lorentz-like line shape. The background is set to the same level for each graph.

dynamical-tunneling-induced dips become more obvious by enhancing the tunneling, as expected.

V. PHYSICAL MEANING OF THE CHAOTIC MODE AND "COMPLETE EXCITATION"

At the beginning of Sec. II, we have presented the chaotic mode $|C_\omega\rangle$. In this section, we will further investigate the meaning of the chaotic mode and the coupling strength to a regular mode $|\mathrm{WGM}\rangle$. To study this case in a general way, we expand the chaotic mode as a linear combination of an orthogonal set at a certain frequency. Using $|C_{\omega(n)}\rangle$ to represent the normalized nth orthogonal mode, we have

$$|C_\omega\rangle = \frac{1}{\sqrt{\sum_n \alpha_{(n)}^2}} \sum_n \alpha_{(n)} |C_{\omega(n)}\rangle, \tag{22}$$

where $\alpha_{(n)}$ stands for the corresponding weight. From the coupled-mode theory, we obtain

$$\dot{\xi}_r = \sum_n g_{(n)} \xi_{(n)}. \tag{23}$$

Here ξ_n and ξ_r represent the electric field of $|C_{\omega(n)}\rangle$ and $|\mathrm{WGM}\rangle$, respectively, with g_n being the coupling strength between them. Thus, the equivalent coupling strength $|V_\omega|$ is derived as

$$|V_\omega| = \frac{1}{\sqrt{\sum_n \alpha_{(n)}^2}} \sum_n \alpha_{(n)} g_{(n)}. \tag{24}$$

Then the reduced coupling strength between $|C_\omega\rangle$ and $|\mathrm{WGM}\rangle$ can be obtained as $\kappa = 2\pi |V_\omega|^2$, according to Eq. (8).

Once the high-Q regular mode $|\mathrm{WGM}\rangle$ is excited, it can dynamically tunnel into all of the chaotic modes, including both $|C_\omega\rangle$ and $|C_\omega^\perp\rangle$. Since the chaotic modes are a continuum, with first Markov approximation, this tunneling can be considered as a spontaneous decay process of the regular mode, described by the coefficient

$$\gamma_\omega = \sqrt{\sum_n g_{(n)}^2}. \tag{25}$$

Thus the decay rate into $|C_\omega^\perp\rangle$ is

$$\frac{\gamma_1}{2\pi} = |\gamma_\omega|^2 - \frac{\kappa}{2\pi} = \frac{\sum_n \alpha_{(n)}^2 \sum_n g_{(n)}^2 - \left(\sum_n \alpha_{(n)} g_{(n)}\right)^2}{\sum_n \alpha_{(n)}^2}. \quad (26)$$

Hence, to optimize the free-space coupling efficiency, according to Cauchy inequality, the coefficients $\alpha_{(n)}$ satisfy

$$\frac{\alpha_{(1)}}{g_{(1)}} = \frac{\alpha_{(2)}}{g_{(2)}} = \cdots = \frac{\alpha_{(n)}}{g_{(n)}}. \quad (27)$$

Under this condition, it is found that $\gamma_1 = 0$. Neglecting the intrinsic loss γ_0 induced by scattering and material absorption, we have $\kappa = \gamma_t$, which means the incident light is exactly a time-reversed way of the emission light from the regular mode $|\mathrm{WGM}\rangle$. It is also in agreement with the second extreme case discussed in Sec. II, in which the "complete excitation" condition requires the incident light as the phase conjugation wave of the emission pattern.

VI. KAM BARRIERS

Finally, we discuss how the KAM tori, behaving as barriers [46,47], can result in a phase shift in dynamical tunneling. This phase shift is crucial to give rise to the Fano resonance. As shown in Fig. 2(a), KAM tori separate the phase space into disconnected regions, between which transport is forbidden classically, but permitted in quantum mechanics [48,49], known as dynamical tunneling. To evaluate the barrier effect, we study the potential of orbits in the PSOS. For the sake of analytical expressions but without loss of the physics, we investigate the orbits in a circular microcavity. The wave function of a WGM with angular momentum number m in circular cavities takes the form

$$\Psi(\mathbf{r},\phi) = f_{\mathrm{m}}(\mathbf{r}) e^{i m \phi}, \quad (28)$$

where $f_{\mathrm{m}}(\mathbf{r})$ satisfies the radial wave equation

$$\left\{-\nabla_{\mathbf{r}}^2 - \frac{[n^2(\mathbf{r})-1]\omega^2}{c^2} + \frac{m^2}{r^2}\right\} f_{\mathrm{m}}(\mathbf{r}) = \frac{\omega^2}{c^2} f_{\mathrm{m}}(\mathbf{r}). \quad (29)$$

Based on the stationary Schrödinger equation,

$$\left(-\frac{\hbar^2}{2\mu}\nabla^2 + V\right) f_{\mathrm{m}}(\mathbf{r}) = E f_{\mathrm{m}}(\mathbf{r}), \quad (30)$$

and substituted with $E = \hbar\omega$, we deduce the effective potential corresponding to the angular momentum number m,

$$V = \frac{\hbar^2}{2\mu}\left\{-\frac{[n(\mathbf{r})^2-1]\omega^2}{c^2} + \frac{m^2}{r^2}\right\}. \quad (31)$$

Extending m to the range of positive real numbers, from the classical relation $m = nkr\sin\chi$ and the nonrelativity approximation $\mu = \hbar\omega/2c^2$, the effective potential of the orbits takes the form

$$V_{\mathrm{eff}}(\sin\chi) = n^2\hbar\omega\sin^2\chi. \quad (32)$$

The effective potentials for different materials (silica and GaAs) are plotted in Fig. 7(a). Thus, a photon at critical

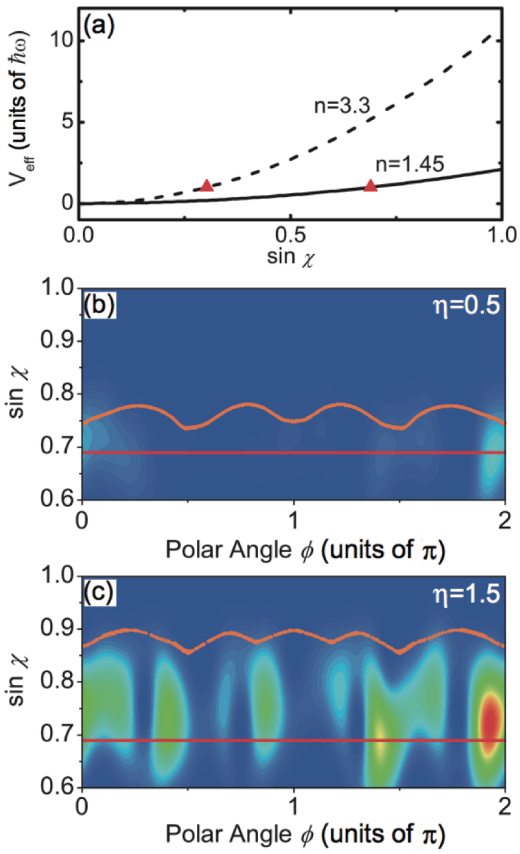

FIG. 7. (Color online) (a) Effective potential V_{eff} against $\sin\chi$. The solid and dashed curves correspond to the cases of silica ($n = 1.45$) and GaAs ($n = 3.3$) microcavities, respectively. The red triangles mark the potential at the critical angle, where the potentials are both $\hbar\omega$. (b), (c) Husimi projections of the excitation state inside the cavity at nonresonant frequency with the deformation parameter η of the cavity setting as 0.5 and 1.5, respectively. These two figures are plotted in the same scale. Orange dotted curves and red solid lines denote KAM tori and critical-refraction lines.

refraction line $\sin\chi = 1/n$ has the same potential as a free-space photon, in agreement with Fresnel's law. The difference in the potentials of various orbits leads to tunneling.

In deformed microcavities, KAM tori are the residue of these invariant orbits, and they perform as barriers in quantum mechanics. By plotting the Husimi projection of cavities of different deformations shown in Figs. 7(b) and 7(c), we can find that the transportation to high-Q modes is governed by the KAM tori. Besides, the intensity of the Husimi projection in Fig. 6(c) is far stronger than that in Fig. 6(b). It reveals that more light is pumped into the cavity with a larger deformation, thus leading to a higher probability to couple into regular high-Q modes.

VII. SUMMARY

In conclusion, we have presented the dynamical tunneling-assisted coupling mechanism to interpret how a free-space laser beam excites the high-Q modes in deformed microcavities. The deformed microcavity has a mixed phase space, where the high-Q regular modes lie in regular regions. The lifetime of

photons refracting into the cavity increases due to chaotic trajectories, which contributes to the enhanced excitation of regular modes via *chaos-assisted dynamical tunneling*. A quantum scattering theory is employed to describe the picture and to obtain the free-space transmission spectra. Unlike evanescent coupling with a waveguide where the transmission spectra behave symmetrically, this model predicts three types of transmission, i.e., asymmetric Fano-like, symmetric EIT-like, and Lorentz dip line shapes, depending on the phase difference related to the fluctuation of background transmission. It is found that the Fano resonance is attributed to the phase shift occurring in the dynamical tunneling into classical-forbidden regions. Our results provide a general method to evaluate the coupling strength between the chaos and the regular mode from the transmission spectra, which can be further extended to the quantitative study of the dynamical tunneling process. The efficient chaos-assisted free-space coupling is of importance to simplify experimental conditions and excite high-Q modes in higher-index-material microcavities.

ACKNOWLEDGMENTS

Q.F.Y. and Y.F.X. thank Kerry Vahala and Fang-Jie Shu for insightful discussions. This work was supported by the 973 program (Grant No. 2013CB328704), the NSFC (Grants No. 11222440, No. 11004003, No. 11023003, and No. 1121091), the RFDPH (Grant No. 20120001110068), and Beijing Natural Science Foundation Program (Grant No. 4132058). Q.F.Y. and Y.L.C. were supported by the National Fund for Fostering Talents of Basic Science (Grants No. J1030310 and No. J1103205) and the Undergraduate Research Fund of Education Foundation of Peking University.

[1] *Optical Microcavities*, edited by K. Vahala (World Scientific, Singapore, 2005).
[2] S.-X. Qian and R. K. Chang, Phys. Rev. Lett. **56**, 926 (1986).
[3] S. M. Spillane, T. J. Kippenberg, and K. J. Vahala, Nature (London) **415**, 621 (2002).
[4] V. S. Ilchenko, A. A. Savchenkov, A. B. Matsko, and L. Maleki, Phys. Rev. Lett. **92**, 043903 (2004).
[5] P. Del'Haye, T. Herr, E. Gavartin, M. L. Gorodetsky, R. Holzwarth, and T. J. Kippenberg, Phys. Rev. Lett. **107**, 063901 (2011).
[6] T. Aoki, B. Dayan, E. Wilcut, W. P. Bowen, A. S. Parkins, T. J. Kippenberg, K. J. Vahala, and H. J. Kimble, Nature (London) **443**, 671 (2006).
[7] Y.-S. Park, A. K. Cook, and H. Wang, Nano Lett. **6**, 2075 (2006).
[8] Y.-F. Xiao, Y.-C. Liu, B.-B. Li, Y.-L. Chen, Y. Li, and Q. Gong, Phys. Rev. A **85**, 031805(R) (2012).
[9] T. J. Kippenberg, H. Rokhsari, T. Carmon, A. Scherer, and K. J. Vahala, Phys. Rev. Lett. **95**, 033901 (2005).
[10] A. H. Safavi-Naeini, T. P. Mayer Alegre, J. Chan, M. Eichenfield, M. Winger, Q. Lin, J. T. Hill, D. E. Chang, and O. Painter, Nature (London) **472**, 69 (2011).
[11] C. Dong, V. Fiore, M. C. Kuzyk, and Hailin Wang, Science **338**, 1609 (2012).
[12] V. Sandoghdar, F. Treussart, J. Hare, V. Lefevre-Seguin, J.-M. Raimond, and S. Haroche, Phys. Rev. A **54**, R1777 (1996).
[13] G. S. Solomon, M. Pelton, and Y. Yamamoto, Phys. Rev. Lett. **86**, 3903 (2001).
[14] L. Yang, D. K. Armani, and K. J. Vahala, Appl. Phys. Lett. **83**, 825 (2003).
[15] Y.-F. Xiao, C.-H. Dong, C.-L. Zou, Z.-F. Han, L. Yang, and G.-C. Guo, Opt. Lett. **34**, 509 (2009).
[16] F. Vollmer, D. Braun, A. Libchaber, M. Khoshsima, I. Teraoka, and S. Arnold, Appl. Phys. Lett. **80**, 4057 (2002).
[17] I. M. White, H. Oveys, and X. Fan, Opt. Lett. **31**, 1319 (2006).
[18] F. Vollmer, S. Arnold, and D. Keng, Proc. Natl. Acad. Sci. USA **105**, 20701 (2008).
[19] J. Zhu, S. K. Ozdemir, Y.-F. Xiao, L. Li, L. He, D.-R. Chen, and L. Yang, Nat. Photon. **4**, 46 (2010).
[20] Y.-F. Xiao, V. Gaddam, and L. Yang, Opt. Express **16**, 12538 (2008).
[21] V. B. Braginsky, M. L. Gorodetsky, and V. S. Ilchenko, Phys. Lett. A **137**, 393 (1989).
[22] J. C. Knight, G. Cheung, F. Jacques, and T. A. Birks, Opt. Lett. **22**, 1129 (1997).
[23] M. Cai, O. Painter, and K. J. Vahala, Phys. Rev. Lett. **85**, 74 (2000).
[24] V. S. Ilchenko, X. S. Yao, and L. Maleki, Opt. Lett. **24**, 723 (1999).
[25] L. Ding, P. Senellart, A. Lemaitre, S. Ducci, G. Leo, and I. Favero, Proc. SPIE **7712**, 771211 (2010).
[26] S.-B. Lee, J. Yang, S. Moon, J.-H. Lee, and K. An, Appl. Phys. Lett. **90**, 041106 (2007).
[27] J. Yang, S.-B. Lee, S. Moon, S. Y. Lee, S. W. Kim, Truong Thi Anh Dao, J.-H. Lee, and K. An, Phys. Rev. Lett. **104**, 243601 (2010).
[28] J. U. Nöckel and A. D. Stone, Nature (London) **385**, 45 (1997).
[29] H. G. L. Schwefel, N. B. Rex, H. E. Tureci, and R. K. Chang, J. Opt. Soc. Am. B **21**, 923 (2004).
[30] Y.-S. Park and H. Wang, Opt. Express **15**, 16471 (2007).
[31] U. Fano, Phys. Rev. **124**, 1866 (1961).
[32] Y.-F. Xiao, X.-F. Jiang, Q.-F. Yang, L. Wang, K. Shi, Y. Li, and Q. Gong, Laser and Photonics Reviews, doi:10.1002/lpor.201300042.
[33] C. L. Zou, F. W. Sun, C. H. Dong, X. W. Wu, J. M. Cui, Y. Yang, G. C. Guo, and Z. F. Han, arXiv:0908.3531.
[34] X.-F. Jiang, Y.-F. Xiao, C.-L. Zou, L. He, C.-H. Dong, B.-B. Li, Y. Li, F.-W. Sun, L. Yang, and Q. Gong, Adv. Mater. **24**, OP260 (2012).
[35] V. I. Arnold, Russ. Math. Surv. **18**, 9 (1963).
[36] J. U. Nöckel, A. D. Stone, and R. K. Chang, Opt. Lett. **19**, 1693 (1994).
[37] C. Gmachl *et al.*, Science **280**, 1556 (1998).
[38] M. Hentschel and K. Richter, Phys. Rev. E **66**, 056207 (2002).
[39] S.-Y. Lee and K. An, Phys. Rev. A **83**, 023827 (2011).
[40] M. Hentschel, H. Schomerus, and R. Schubert, Europhys. Lett. **62**, 636 (2003).
[41] As the regular mode lies on an invariant torus behaving much like whispering gallery mode, we use WGM to represent it.
[42] A. Bäcker, R. Ketzmerick, S. Löck, and L. Schilling, Phys. Rev. Lett. **100**, 104101 (2008).

[43] C. W. Gardiner and P. Zoller, *Quantum Noise*, 3rd ed. (Springer, Berlin, 2004).
[44] H. Schomerus and M. Hentschel, Phys. Rev. Lett. **96**, 243903 (2006).
[45] J. Yang, S.-B. Lee, S. Moon, S.-Y. Lee, S. W. Kim, and K. An, Opt. Express **18**, 26141 (2010).
[46] T. Geisel, G. Radons, and J. Rubner, Phys. Rev. Lett. **57**, 2883 (1986).
[47] I. I. Rypina, M. G. Brown, F. J. Beron-Vera, H. Kocak, M. J. Olascoaga, and I. A. Udovydchenkov, Phys. Rev. Lett. **98**, 104102 (2007).
[48] J.-B. Shim, S.-B. Lee, S. W. Kim, S.-Y. Lee, J. Yang, S. Moon, J.-H. Lee, and K. An, Phys. Rev. Lett. **100**, 174102 (2008).
[49] Q. Song, L. Ge, B. Redding, and H. Cao, Phys. Rev. Lett. **108**, 243902 (2012).